Sound waves and angular orientation in fibrous materials

H T Luu, C. Perrot, V Monchiet, R. Panneton

▶ To cite this version:

HAL Id: hal-01663980

https://hal.science/hal-01663980

Submitted on 18 Dec 2017

Sound waves and angular orientation in fibrous materials

H. T. Luu [1,2]**, C. Perrot** [2]**, V. Monchiet** [2]**, R. Panneton** [1]

[1] Groupe d'Acoustique de l'Université de Sherbrooke (GAUS), Department of Mechanical Engineering, Université de Sherbrooke, Québec J1K 2R1, Canada,

[2] Université Paris-Est, Laboratoire Modélisation et Simulation Multi Echelle, MSME UMR 8208 CNRS, 5 bd Descartes, 77454 Marne-la-Vallée, France,

e-mail: hoang.tuan.luu@usherbrooke.ca, camille.perrot@u-pem.fr

Abstract

Angular orientation is a state of fibers which can be intentionally changed to modify the properties of the corresponding material. Here, the angular orientation tensor of a fibrous material is identified from scanning electron microscope images, in order to construct a model of the microgeometry, in which the partial differential equations governing the physics at the upper scale can be solved. Permeability and impedance tube measurements show that the corresponding model is a good candidate to simulate the transport properties of fibrous materials. It is also shown that the transport properties of the samples are highly affected and tunable through the angular orientation of the fibers. The proposed numerical approach can be applied to evaluate the effective transport and sound absorbing properties of general fibrous materials just from the geometrical information embodied in the microstructural parameters of single fibers, the fibers orientation distribution and the bulk porosity.

1 Introduction

Direct determination of the effective transport and acoustical properties of disordered porous media from their microstructure is a problem receiving increasing attention as materials are constantly evolving to meet specific requirements. A wide class of naturally occurring and synthetic porous media is composed of fibers with different diameters and angular orientations. Typical examples of these media include mineral wools (glass, rock) or webs made from petro-sourced (polyester, polypropylene) and natural fibers (wood, hemp, cellulose). Due to the random complex geometry of real non-woven fibrous materials, an exact analytical prediction of the effective properties cannot be made, except for idealistic morphology.[1] An attractive alternative is given by the self-consistent method which encapsulates the essential parts of the physics and reduces the morphology of a porous media to the most basic geometrical information, i. e., the porosity and the pore size.[2,3] Disordered porous materials can also be studied by using n-point probability functions in order to correlate the geometrical microstructure of a heterogeneous material with its effective physical properties.[4,5] Another fruitful path has been the development of a random-generation growth algorithm for reproducing multiphase microstructures combined with a lattice Boltzmann solver.[6] Studies starting from first-principle calculations in porous media derived through the application of the numerical homogenization procedure appear to open-up new possibilities[7] for the sake of linking structure and acoustic properties and have attracted much attention. Interestingly, despite the variability of the microstructures, all the numerical data are shown to satisfy approximate scaling relations based on universal functions independent of microstructures.[8,9] By calculating asymptotic constants (viscous permeability k_0, viscous characteristic length Λ, tortuosity σ_∞, and thermal permeability k_0') of porous media models, based on the resolution of three boundary value problems, the long wavelength frequency-dependent acoustic properties of real porous media, yet disordered, may be

inferred with reasonable accuracy.

Permeability is a key parameter for predicting sound waves properties of fibrous materials. The first ab initio simulations of creeping flow through large three-dimensional random fiber webs that closely resemble fibrous sheets, such as paper and nonwoven fabrics, were proposed by Koponen *et al.*[10] Other researchers showed that calculations could be performed for several sets of fiber networks with different degrees of alignment. The result provides a method to estimate permeabilities of anisotropic random networks based only on the distribution of fibers.[11] Tahir and Tafreshi also reported results of simulations showing that transverse permeability increases with increasing the deviation of the fibers' through-plane angle from zero.[12] Tamayol *et al.* also analyzed the impact of the orientation of fibers on the effective permeability and Forchheimer coefficient in random or regular packings of monodispersed fibers at moderate Reynolds number.[13] Results suggesting that permeability and Forchheimer coefficient are functions of porosity and fiber orientation are successfully compared with experimental data. Recently, Soltani *et al.* employed digital image processing techniquess[14] to identify the fiber orientation tensor of real fibrous samples from their three-dimensional images using X-ray micro-computed tomography. The authors utilized the fiber orientation tensor to reconstruct random models from which they can predict the effective permeability by numerical simulations.[15] None of the above referenced studies considers the effect of fiber orientation on sound waves and we address that issue in this work.

The general objective of this paper is to determine the geometrical properties, the permeability and the acoustical properties of real fibrous materials whose local geometry parameters of the microstructure are identified by scanning electron micrograph (SEM) images. Also, the angular orientation of the fibers in the modeled sample is subjected to strong modifications and the overall transport and acoustical properties are determined for different degrees of alignment of fibers. The literature directly related to this subject can be summarized as follows. The authors of Ref.16 conducted permeability simulations on fibrous materials consisting in a spatially stationary system of lines (Poisson line process), dilated by a sphere. Two-dimensional (2D) microscopic images of cross-sections are used to identify the anisotropy of the model described by a one parametric distribution of fibers. The flow is then computed in stochastic realizations of the geometric model using the lattice Boltzmann method. The empirical formulas of Delany and Bazley[17] are then used to estimate the frequency-dependent acoustic absorption of the samples. The permeability of the geometric model leading to the best acoustic absorption was also identified. The authors of Ref.18 simulated transport properties of a P-wave propagating through a 2D porous media made from cylindrical inclusions. This contribution was completed by a double porosity analysis of these particles.[18] The authors of Ref.19 used finite element simulations over periodic unit cells of randomly distributed fibers. However, we would argue that they used a Boolean model of overlapping discs determined according to a random Poisson point process, which means that means that the model is also limited to 2D numerical simulations. They applied it to a fibrous material made from wood fibers, whose morphological properties were highlighted (with a porosity of about = 0.64, and a weighted average radius = 42 μm).[20] The acoustic simulation is made along the Oz axis, perpendicularly to the fibers which are isotropically oriented in the xOy plane. By contrast with previous works,[22] the homogenized acoustic absorption coefficient is obtained without any experimental fitting from measurements.

Wang *et al.*[21] employed the random generation-growth method to produce the structure of carbon fiber composites and to predict their effective thermal conductivity. The structure generation process requires the knowledge of a fiber number density. The determination of the orientation angles for each fiber is defined through the assignment of random number pairs for the 3D case, and each fiber is grown from the core along the assigned direction until the fiber length reach the specified value or the volume fraction of fibers attains a given level. Here, we utilize an alternative approach to generate the fibers. It comprises the adaptation of the algorithm of Wang et al. for the numerical determination of the number of fibers in the REV when the fibers are long and their diameters are known. The present work extends the approach of Venegas and Umnova[18] and Peyrega and Jeulin[19] in three dimensions for geometries of rigid cylinders. Unlike the studies conducted by the authors of Ref.11−13,15 which focus on the effect of 3D fiber orientation on permeability of realistic fibrous networks, we include the inertial and thermal effects in the physics of the simulated acoustic porous materials, and validates the resulting properties against experimental measurements.

The investigation presented here has two specific objectives. First, to introduce and validate our 3D representative elementary volumes (REV). Second, to test the validity of fiber orientation tensor models for the prediction of acoustic properties. In the following, the microstructural characteristics of the fibrous media are identified from scanning electron microscopy, and the macroscopic properties (viscous fluid flow, non-viscous fluid flow, heat conduction) are calculated in the three-dimensional reconstructed sample. In addition, the macroscopic properties are calculated with a systematic variation in the orientation of fibers (from non-aligned to aligned fiber networks). The numerical predictions are compared with experimental measurements (permeability and impedance tube data) performed on the same piece of material.

The paper is organized as follows. The numerical methodology is presented in Sec.**2**. The measurement procedure is briefly described in Sec.**2.1**. The results serve for the generation procedure of fibrous materials. The numerical results and their comparison with experimental data are given in Sec.**3**. First, the transport and acoustical properties of the reconstructed fibrous samples are determined; second, the elastic properties are identified by inversion and the sound transmission loss is derived. The results are compared with experimental data and discussed.

2   Numerical methods

2.1   Generation of random fibrous materials

The investigated non-woven fibrous materials used in this study are considered to be a disordered structure of fibers randomly distributed in a three-dimensional space and assumed to interpenetrate at the crossovers. We considered the fibers to be circular cylinders. The generation scheme is similar to the algorithm of Wang et al. An initial number of fiber core positions is chosen in relation with a given fiber number density. The geometrical characteristics of the cylinders in the generated fiber-webs were modeled after the experimentally determined fiber diameters and proportion of each type of fibers [natural fibers (fiber type a) and petro-sourced fibers (fiber type b) used as a thermal binder. All the structures were generated for a given porosity ($\phi = 0.962 \pm 0.004$ which corresponds to the measured porosity).[23] The same generating protocol was

	Asclepias fibers (a)	Bicomponent fibers (b)
Fiber lengths		
Number of measured fiber segments	1959	1140
Fiber segments cumulated length (L), μm	467840	173820
Fiber diameters		
Number of measured fibers	744	184
Mean diameter (d), μm	25	14.7
Standard deviation (σ_d), μm	6.6	1.7
Fiber wall thicknesses		
Number of measured fibers	119	-
Mean thickness (t), μm	1.6	-
Standard deviation (σ_t), μm	0.4	-
Fiber vertical orientation angles		
Number of measured fibers	3322	
Mean angle (μ_θ) $degree$	89.73	
Standard deviation (σ_θ) $degree$	13.63	
Min. angle θ_{min}, $degree$	0.00	
Max. angle θ_{max}, $degree$	166.53	

Table 1: Statistical properties of the experimentally determined geometrical characteristics of fibers from SEM images.

followed for all fiber-webs. This approach enables to capture the effect of the angular orientation at consistent porosity or the effect of porosity at consistent angular orientation.

Random fibrous materials were generated based on the geometrical characteristics of a porous material made from seed fibers of Asclepias Syriaca (milkweed floss). The internal and external diameters of hollow fibers were estimated by scanning electron microscopy (SEM). A S-3000N scanning electron microscope (Hitachi, Tokyo, Japan) was used to acquire 28 images of horizontal (xy-plane) and 28 images of vertical (orthogonal of the xy-plane) cross-sections, at different locations of the porous material made from Asclepias fibers, among which 3601 and 3322 fiber orientation angles, respectively, were manually measured. Afterwards, the experimental data were converted into continuous probability density functions using uniform and normal estimates. The experimental histograms and the resulting probability density functions are shown in Fig.1. These two types of cross-section are characterized by different behaviors of their angular orientations. The probability density function corresponding to SEM images taken along the horizontal plane is uniform; whereas the angular orientation of fibers corresponding to SEM images taken along the vertical plane is characterized by a mean orientation angle $\mu_\theta = 89.73°$ and a standard deviation $\sigma_\theta = 13.63°$. The statistical properties of the experimentally determined geometrical characteristics from SEM images are summarized in Table 1. Note that the ratio between the fibers cumulated length and the number of measured fibers, equal to 238 μm, corresponds to the average length of measured fiber segments under SEM images; and not to the typical length of natural fibers, this later being on the order of 2 to 4 cm. Next, the computations are made on a Periodic Unit Cell (PUC) as the REV. The PUC resembles a cubic box with dimension $L^{(i)}$ for
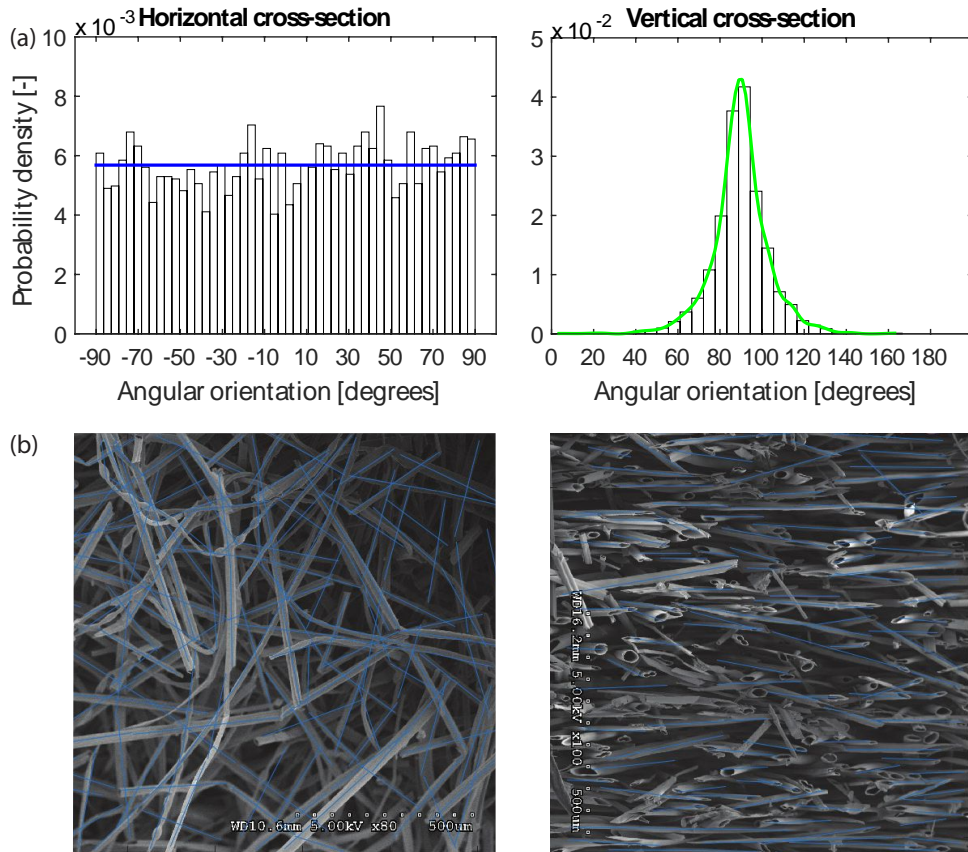

Figure 1: (a) Fiber orientation distributions as experimentally determined by scanning electron microscopy. Histograms were converted into probability density functions. (b) Scanning electron microscope images corresponding to horizontal (x-y plane) and vertical (orthogonal to x-y plane) cross-sections at a porosity $\phi = 0.962 \pm 0.004$. Blue segments characterize the lengths and orientations of the fibers, as manually measured.

iteration *i*. We recall that *a* and *b* account for two different fiber types, i.e., Asclepias and bicomponent (synthetic) fibers respectively. By determining the total fibers volumes $V_a^{(i)}$ and $V_b^{(i)}$ inside the elementary volume *(i)*, it is possible to compute the number of fibers $N_a^{(i)}$ and $N_b^{(i)}$, and derive porosity ϕ^i as well as thermal characteristic length Λ'^i also known as generalized hydraulic radius. In our case, the values of $V_a^{(i)}$ and $V_b^{(i)}$ are defined analytically from the targeted (final) porosity ϕ, the cubic box volume $L^{(i)3}$, the fiber radii r_a and r_b, the wall thickness t, and the ratio between bicomponent and Asclepias fibers L_b/L_a.

$$V_a^{(i)} = \frac{(1-\phi)L^{(i)3}}{1 + \frac{L_b}{L_a} \times \frac{r_b^2}{r_a^2-(r_a-t)^2}}, \qquad V_b^{(i)} = \frac{L_b}{L_a} \times \frac{r_b^2}{r_a^2 - (r_a - t)^2} \times V_a. \qquad (1)$$

Figure 2: Iterative procedure to calculate the cubic box dimension and the number of fibers for the given fibrous material geometrical characteristics and porosity.
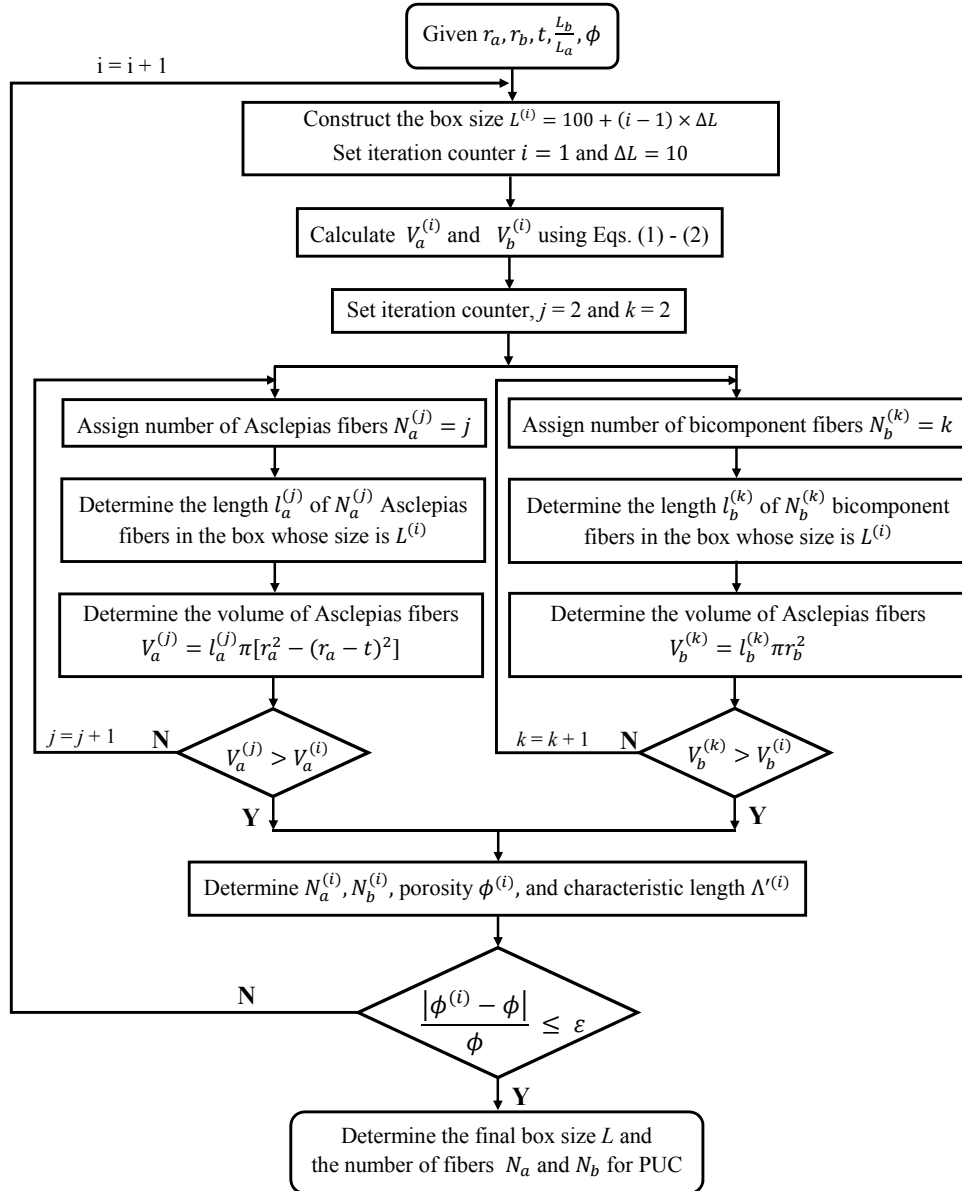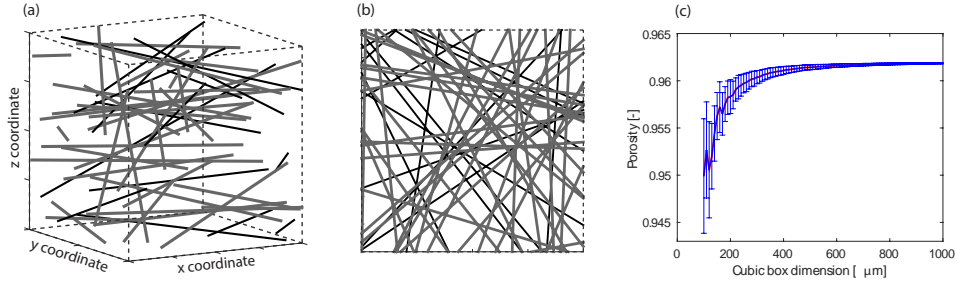
Figure 3: Iterative procedure to calculate the cubic box dimension and the number of fibers for the given fibrous material geometrical characteristics and porosity.

Then, the iterative determination of the number of fibers $N_a^{(i)}$ and $N_b^{(i)}$ starts by considering a three-dimensional and two-phased (fiber/air) fibrous material (whose internal structure is shown in Fig.1(b), left). Each iteration consists of three sequential steps: (i) randomly locate the fiber core c_j of position (x_j, y_j, z_j) according to a uniform distribution; (ii) randomly assign orientation angles θ_j and φ_j to the fiber core c_j, the orientation angle of the fiber can be any value within $[0, \pi[$ and $[-\pi/2, \pi/2[$; (iii) calculate the fiber length l_j inside the cubic of side $L^{(i)}$, from which the elementary solid volumes are derived for each type of fibers (nested loops). As the sums of these elementary solid volumes asymptotically approach $V_a^{(i)}$ and $V_b^{(i)}$, the current porosity $\phi^{(i)}$ approach ϕ. The number of iterations i defines the number of fibers $N_a^{(i)}$ and $N_b^{(i)}$. This procedure essentially allows iterative alteration of the cubic box dimension $L^{(i)}$ until porosity is converged. The implemented algorithm is depicted in Fig.2. Applying it for 1000 cases corresponding to each box size resulted in a minimum mean value of the parameter L equal to 400μm, to obtain a relative porosity difference between the experimental and calculated values of less than $\varepsilon = 0.1\%$. The program realization of the box-size-algorithm was implemented as a parallel code in Matlab language. The total simulation time was ~ 163 s on 3.47Ghz/8 processor cores (160 Go memory). Fig.3 shows the corresponding (a) three-dimensional and (b) front view of a generated fiber packing at a porosity $\phi = 0.962$. In these illustrations, the grey lines define the Asclepias fibers, whereas the black ones account for the bicomponent fibers. As the cubic box dimension iteratively increases, the porosity asymptotically approaches the targeted (experimental) porosity ϕ while reducing the standard deviation; Fig.3(c).

2.2 Simulation of transport properties

Similar to our previous paper,[24] Stokes flow, potential flow, and heat conduction in the generated fiber webs were simulated using a finite element (FEM) scheme. The permeability k_0 for the Stokes flow was obtained by averaging the velocity components in the direction of the flow. Similarly, the "thermal permeability" k_0' satisfies the mean value of the "scaled concentration field" $\overrightarrow{u}_p(r)$, where $\overrightarrow{u}_p(r)$ solves $\Delta u_p = -1$ in the pore space V_p and $\overrightarrow{u}_p(r) = 0$ on the pore walls A. Then, the quantities Λ and α_∞ were calculated from the definitions as

$$\alpha_\infty = \frac{\phi A |\Psi_L|^2}{L \int |\overrightarrow{u}_p(r)|^2 dV}, \qquad \Lambda = 2\frac{\int |\overrightarrow{u}_p(r)|^2 dV}{\int |\overrightarrow{u}_p(r)|^2 dA}, \qquad (2)$$

see Ref.8, equations (2.9) and (2.17). The quantities and denote viscous characteristic length and tortuosity,[25] respectively. It can be demonstrated that α_∞ magnitude is greater or equal to one and the equality takes place only if the pore space is a bundle of straight channels. In Eqs. 2, $\overrightarrow{u}_p(r)$ stands for the anti-gradient of the potential

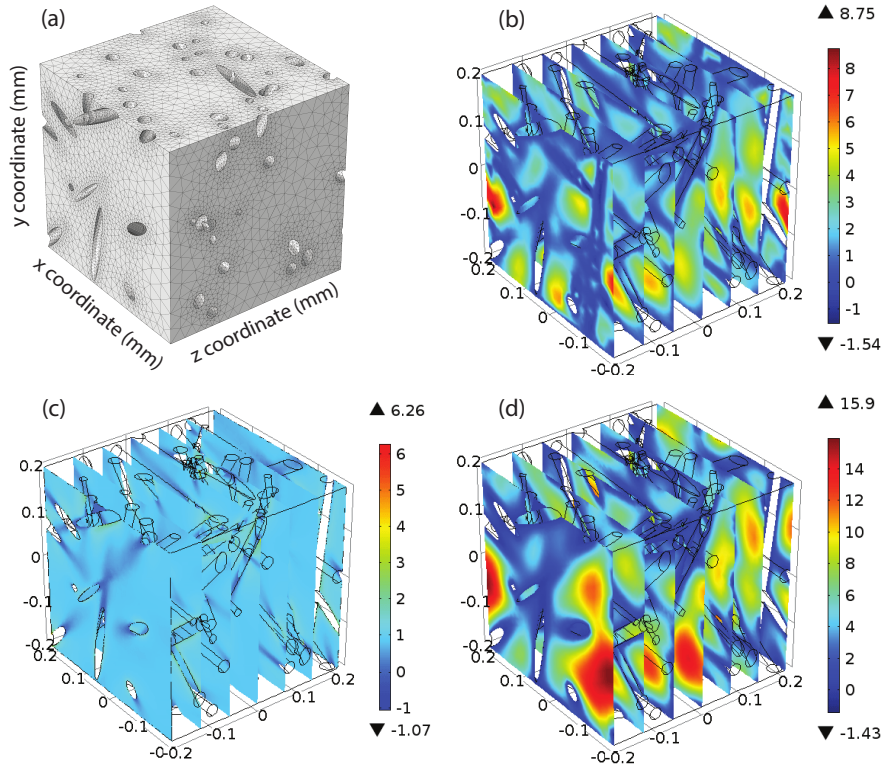$$\overrightarrow{u}_p(r) = -\overrightarrow{\nabla}\Psi. \qquad (3)$$

Figure 4: Asymptotic fields for the reconstructed representative elementary volume: (a) Mesh domain corresponding with 497 909 elements, (b) scaled velocity field corresponding to Stokes flow in z direction $[\times 10^{-11} \text{m}^2]$, (c) scaled velocity field corresponding to potential flow in the z direction [-], (d) scaled heat diffusion field $[\times 10^{-11} \text{m}^2]$.

Here, Ψ was the solution to Laplace equation subjected to boundary condition $\Psi = \Psi_L$ at the outlet, $\Psi = 0$ at the inlet boundary, and the potential drop between the inlet and outlet boundaries was equal to Ψ_L. At the pore walls inside the medium, the potential Ψ satisfied Neumann condition $\partial \Psi / \partial \overrightarrow{n} = 0$, where $\overrightarrow{n}$ is the surface normal. The boundary conditions for the potential flow were selected to have a unit potential drop across the opposite face of the sample. From the Stokes flow problem, we set $p = 0$ for the pressure on the opposite faces of the sample and added a unit constant body force along the direction of the flow. In this numerical study, we considered only solid fibers. We generated a tetrahedralization of the pore space. The obtained tetrahedralization was then used to create a finite element mesh for the COMSOL Multiphysics[26] Stokes and Laplace solvers. For all the numerical schemes, the flow was evaluated in direction z. Simulations were carried out according to periodic boundary conditions. Fig.4 shows the solution fields evaluated by FEM numerical solutions for flows and diffusion in the z direction. Note that visually the fluid-flow paths are clearly more concentrated and follow a more tortuous path due mainly to the no-slip boundary condition than do the potential velocity paths. Moreover, as already mentioned by Boutin and Geindreau[3] the heat diffusion field is independent of the orientation of the fibers (it can be viewed as the superposition of the flow field in the three main directions). The typical simulation times for Stokes flow, potential flow, and heat diffusion problems of transport are, respectively, equal to 442 ± 47 s, 14 ± 2 s, and 15 ± 2 s (using a computer with a 3.40 GHz processor core and a 24 Go memory).

2.3 Estimation of acoustic properties

Based on the approximate formulae developed by Johnson *et al.*[8] and Lafarge *et al.*,[9] the effective density $\rho_{eff}(\omega)$ and the effective bulk modulus $K_{eff}(\omega)$ of the fluid phase can be evaluated as follows:

$$\rho_{eff}(\omega) = \rho_0 \alpha_\infty \left[1 + \frac{1}{\overline{\omega}} f(\overline{\omega}) \right], \tag{4}$$

$$\frac{1}{K_{eff}(\omega)} = \frac{1}{K_a} \left\{ \gamma - (\gamma - 1) \left[1 + \frac{1}{j\overline{\omega}'} f'(\overline{\omega}') \right]^{-1} \right\}, \tag{5}$$

where ρ_0 is the air density at rest, K_a is the adiabatic bulk modulus of air and γ is its specific heat ratio. The quantities $\overline{\omega}$ and $\overline{\omega}'$ are dimensionless frequencies given by the following expressions:

$$\overline{\omega} = \frac{\omega}{\nu} \frac{k_0 \alpha_\infty}{\phi}, \qquad \overline{\omega}' = \frac{\omega}{\nu} \frac{k_0'}{\phi}, \tag{6}$$

with $\nu' = \nu/Pr$, ν being the kinematic viscosity and Pr is the Prandtl number. $f(\overline{\omega})$ and $f'(\overline{\omega}')$ are shape functions defined by

$$f(\overline{\omega}) = \sqrt{1 + \frac{M}{2} j\overline{\omega}}, \qquad f'(\overline{\omega}) = \sqrt{1 + \frac{M'}{2} j\overline{\omega}'}, \tag{7}$$

M and M' are referred to as dimensionless shape factors determined from

$$M = \frac{8k_0 \alpha_\infty}{\Lambda^2 \phi}, \qquad M' = \frac{8k_0'}{\Lambda'^2 \phi}. \tag{8}$$

$\rho_{eq}(\omega) = \rho_{eff}(\omega)/\phi$ and $K_{eq}(\omega) = K_{eff}(\omega)/\phi$ are the effective density and bulk modulus of the so-called rigid-frame equivalent fluid medium. Looking from plane wave solutions varying as $\exp[j(\omega t - q_{eq}(\omega)x)]$, where $q_{eq}(\omega)$ represents the wave number of the equivalent fluid medium, $\rho_{eq}(\omega)$ and $K_{eq}(\omega)$ can be used to calculate the wave number and the characteristic impedance of the equivalent fluid medium with:

$$q_{eq} = \omega \sqrt{\frac{\rho_{eq}(\omega)}{K_{eq}(\omega)}}, \qquad Z_{ceq} = \sqrt{\rho_{eq}(\omega) K_{eq}(\omega)}. \tag{9}$$

The sound absorption coefficient at normal incidence of a porous material layer of thickness d backed by a rigid wall is evaluated by

$$\alpha = 1 - \left| \frac{Z_n - 1}{Z_n + 1} \right|^2, \qquad with \qquad Z_n = -j \frac{Z_{ceq}}{Z_0} \cot(q_{eq}d), \tag{10}$$

the effective normal impedance on the free face of the excited material, where Z_0 is the characteristic impedance of ambient air. Then, the normal incidence transmission coefficient τ_∞ is determined from the equivalent wave number and the equivalent characteristic impedance of the acoustical material as

$$\tau_\infty = \frac{2e^{q_0 d}}{2\cos(q_{eq}d) + j\frac{Z_{ceq}}{Z_0} + j\frac{Z_{ceq}}{Z_0}\sin(q_{eq}d) + j\frac{Z_0}{Z_{ceq}}\sin(q_{eq}d)}. \tag{11}$$

Finally, the normal incidence sound transmission loss is obtained from

$$TL = -20\log(|\tau_\infty|). \tag{12}$$

When the frame of the porous material is assumed limp (i.e. flexible), the effective density is modified as follows:[29]

$$\rho_{eq}'(\omega) = \frac{\rho_{eq}(\omega)m - \rho_0^2}{m + \rho_{eq}(\omega) - 2\rho_0}, \tag{13}$$

where $m = \rho_1 + \phi\rho_0$ is the total apparent mass of the equivalent fluid limp medium, ρ_1 is the *in vacuo* bulk density of the medium.

3   Results and discussion

In Table 2, we present the computed values of transport parameters for the Asclepias/bicomponent fiber assembly having the measured porosity of $\phi = 0.962 \pm 0.004$, an *in vacuo* bulk density of $\rho_1 = 32.30 \pm 0.07$ $kg.m^{-3}$, and the fiber orientation distributions identified according to Fig.1. In practice, we employed the proposed numerical approach to generate random webs of solid fibers. Realization of such geometrical configurations assumes that the hollow effect of fibers does not significantly influence the effective acoustic behavior at first order. As a result, the fluid volume fractions of the simulated solid fiber webs are equal to 0.900 ± 0.003. The numerically determined is very close to the corresponding experimental value.[28] Good agreements were also observed for the acoustic properties presented in Fig.5. We notice that all of the proposed models (rigid,[8,9] limp,[29] elastic[30]) predict an overall sound absorption in agreement with measurements.

In the rigid case, the model used was the Johnson-Lafarge one presented throughout Sec. 2.3 with the computed parameters given in Table 2 ($\phi = 0.900$ for the above mentioned reasons). We also used the limp model in which the effective density of the rigid-frame equivalent fluid medium is corrected according to Eq. 13. In the elastic case, an axisymmetrical finite element poroelastic model was used. In this model, the same $\rho_{eq}(\omega)$ and $K_{eq}(\omega)$ as described in Sec. 2.3 were used for the fluid phase. For the solid phase, the elastic properties were adjusted so that the predictions better fit both the measured absorption and transmission curves. Moreover, to better replicate the mounting conditions of the sample in the tube, the axial motion was constrained on its edge in the FE model: due to friction, the contour of the sample was constrained in the tube. It can be seen from Fig.5(b) that only an elastic model enables to achieve a full coverage of both the sound absorption and the sound transmission predictions. The adjusted elastic properties of the corresponding poro-elastic fibrous samples are $E = 280000\ N.m^{-2}$, $\nu = 0$, $\eta = 0.01$; where E, ν, and η respectively account for the Young's modulus, Poisson's ratio, and damping loss factor of the bounded samples inside an impedance tube of 44.5 mm in diameter. This triplet of parameters represents a physically realistic elastic behavior for a fibrous, yet bounded material: the Young's modulus may appear at a first sight as being relatively high when compared to standard fibrous materials, but this has to be attributed as explained before to an effective rigidity due to boundary conditions. The values corresponding to the remaining elastic parameters, ν and η, are classical for fibrous materials. It is clear that these elastic properties are to be computed from the application of the numerical homogenization procedure, too. This should be the tentative topic of a forthcoming paper.

The main conclusion which can be drawn from the data presented in Table 2 and Fig.5 is that the use of the generated random fibrous material reconstructed from the experimentally determined: (i) geometrical characteristics of single fibers, (ii) probability density functions for angular orientations, and (iii) porosity; allows to estimate accurately the transport and the acoustical properties of the sample we analyzed in this study. Thus, the proposed approach allows to get a good estimate of the acoustic properties of random fibrous

| | ϕ (-) | | $\Lambda^{'}$ | α_∞ | Λ | k_0 | $k_0^{'}$ |
	hollow fibers	solid fibers	(μm)	(-)	(μm)	($\times 10^{-11} m^2$)	($\times 10^{-11} m^2$)
Measurements	0.962					19.571	
	± 0.004					± 1.184	
Computations	0.963	0.900	103	1.054	51	19.247	61.838
	± 0.003	± 0.003	± 4	± 0.003	± 2	± 0.892	± 5.848

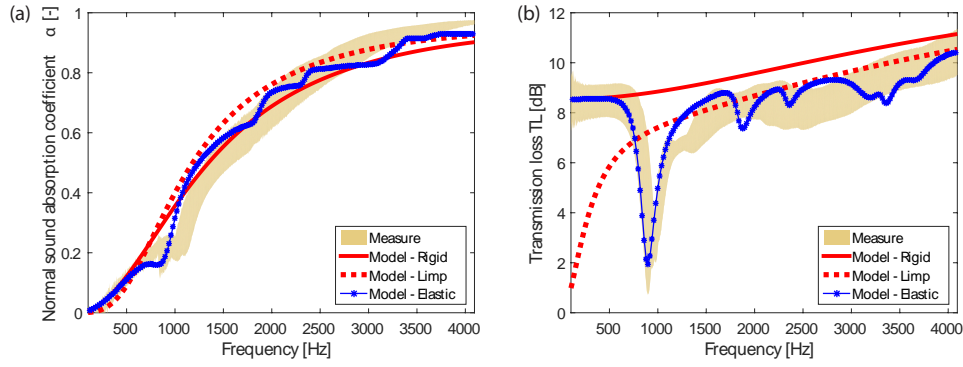Table 2: Macroscopic parameters: measurements and computational results.

Figure 5: Comparison between measurements and prediction: (a) normal incidence sound absorption coefficient, (b) transmission loss. The sample thickness is equal to $14.30 \pm 0.89 mm$.

materials, using only information of fibrous network geometry.

4 Conclusions

This work reports on results obtained for elementary transport phenomena in random fibrous media. Fibrous media used as sustainable acoustic materials with a porosity of $\phi = 0.962 \pm 0.004$ were computer-generated at a fixed generation protocol based on experimentally measured fiber orientation distribution estimated by scanning electron microscopy.

The calculation of transport properties was carried out using a finite element scheme. It involves the Stokes flow, potential flow, and diffusion controlled reactions, which can be solved routinely in the reconstructed fibrous samples. Our results demonstrate that the values of the transport and acoustic coefficients in the investigated fiber webs are determined by their porosity ϕ, the geometrical characteristics of the constitutive fibers, and by the degree of alignment of fibers as compared to the direction of wave propagation. The permeability coefficient computed by FEM was compared with k_0 values derived from direct standard measurements in the reconstructed fibrous sample, with a good agreement. The use of the remaining transport coefficients allows determining estimates of acoustic properties directly from information on the geometrical structure of a fiber web. The generalization and automatization of the approach to a large class of fibrous materials will be part of our further work. Extension to elastic properties will require the modeling of the connections between fibers. The proposed approach is extendable to any physical property of fibrous media in principle. Thus, the presented approach provides a straightforward routine to evaluate the effective properties of fibrous media and to analyze structure-property-manufacturing relationships in general.

5 Acknowledgements

References

[1] V. Tarnow, *Airflow resistivity of models of fibrous acoustic materials*, Journal of the Acoustical Society of America, Vol. 100 (1996), pp. 3706-3713.

[2] M. Thiery and C. Boutin, *Poromechanics II*, Edited by J. Auriault et al. Balkema, The Netherlands (2002), pp. 575-581.

[3] C. Boutin and C. Geindreau, *Periodic homogenization and consistent estimates of transport parameters through sphere and polyhedron packings in the whole porosity range*, Physical Review E, Vol. 82 (2010), pp. 036313 (1-18).

[4] P. B. Corson, *Correlation functions for predicting properties of heterogeneous materials. I. Experimental measurement of spatial correlation functions in multiphase solids*, Journal of Applied Physics, Vol 45 (1974), pp. 3159-3164.

[5] D. Hlushkou, H. Liasneuski, U. Tallarek, and S. Torquato, *Effective diffusion coefficients in random packings of polydisperse hard spheres from two-point and three-point correlation functions*, Journal of Applied Physics, Vol. 118 (2015), pp. 124901 (1-10).

[6] M. Wang and N. Pan, *Predictions of effective physical properties of complex multiphase materials*, Materials Science and Engineering R, Vol. 63 (2008), pp. 1-30.

[7] M.-Y. Zhou and P. Sheng, *First-principles calculations of dynamic permeability in porous media*, Physical Review B, Vol. 39, No. 16 (1989), pp. 12027-12039.

[8] D. L. Johnson, J. Koplik and R. Dashen, *Theory of dynamic permeability and tortuosity in fluid-saturated porous media*, Journal of Fluid Mechanics, Vol. 176 (1987), pp. 379-402.

[9] D. Lafarge, P. Lemarinier, J. F. Allard, and V. Tarnow, *Dynamic compressibility of air in porous structures at audible frequencies*, Journal of the Acoustical Society of America, Vol. 102 (1997), pp. 1995-2006.

[10] A. Koponen, D. Kandhai, E. Hellén, M. Alava, A. Hoekstra, M. Kataja, K. Niskanen, P. Sloot, and J. Timonen, *Permeability of three-dimensional random fiber webs*, Physical Review Letters, Vol. 80 (1998), pp. 716-719.

[11] T. Stylianopoulos, A. Yeckel, J. J. Derby, X.-J. Luo, M. S. Shephard, E. A. Sander, and V. H. Barocas, *Permeability calculations in three-dimensional isotropic and oriented fiber networks*, Physics of Fluids, Vol. 20 (2008), pp. 123601 (1-10).

[12] M. A. Tahir and H. V. Tafreshi, *Influence of fiber orientation on the transverse permeability of fibrous media*, Physics of Fluids, Vol. 21 (2009), pp. 083604 (1-5).

[13] A. Tamayol, K. W. Wong, and M. Bahrami, *Effects of microstructure on flow properties of fibrous porous media at moderate Reynolds number*, Physical Review E, Vol. 85 (2012), pp. 026318 (1-7).

[14] H. Yang, W.B. Lindquist, *Three-dimensional image analysis of fibrous materials*, *Proceedings of The SPIE: Applications of digital image processing, San Diego, USA, 2000*, San Diego, USA, 2000, pp. 275-282.

[15] P. Soltani, M. S. Johari, M. Zarrebini, *Effect of 3D fiber orientation on permeability of realistic fibrous porous networks*, Powder Technology, Vol. 245 (2014), pp. 44-56.

[16] K. Schladitz, S. Peters, D. Reinel-Bitzer, A. Wiegmann and J. Ohser, *Design of acoustic trim based on geometric modeling and flow simulation for non-woven*, Computational Materials Science, Vol. 38 (2006), pp. 56-66.

[17] M. E. Delany and E. N. Bazley, *Acoustical properties of fibrous absorbent materials*, Applied Acoustics, Vol. 3 (1970), pp. 105-116.

[18] R. Venegas and O. Umnova, *Acoustical properties of double porosity granular materials*, Journal of the Acoustical Society of America, Vol. 130 (2011), pp. 2765-2776.

[19] C. Peyrega and D. Jeulin, *Estimation of acoustic properties and of the representative volume element of random fibrous media*, Journal of Appied Physics, Vol. 113 (2013), pp. 104901 (1-13).

[20] C. Peyrega, D. Jeulin, C. Delisée and J. Malvestio, *3D morphological characterization of phonic insulation fibrous media*, Advanced Engineering Materials, Vol. 13, No. 3 (1987), pp. 156-164.

[21] M. Wang, Q. Kang, N. Pan, *Thermal conductivity enhancement of carbon fiber composites*, Applied Thermal Engineering, Vol. 29 (2009), pp. 418-421.

[22] K. Attenborough, *Acoustical characteristics of rigid fibrous absorbents and granular materials*, Journal of the Acoustical Society of America, Vol. 73 (1983), pp. 785-799.

[23] Y. Salissou and R. Panneton, *Pressure/mass method to measure open porosity of porous solids*, Journal of Applied Physics, Vol. 101 (2007), pp. 124913 (1-7).

[24] C. Perrot, F. Chevillotte, M. T. Hoang, G. Bonnet, F. X. Bécot, L. Gautron and A. Duval, *Microstructure, transport, and acoustic properties of open-cell foam samples: Experiments and three-dimensional numerical simulations*, Journal of Applied Physics, Vol. 111 (2012), pp. 014911 (1-16).

[25] R. J. Brown, *Connection between formation factor for electrical resistivity and fluid-solid coupling factor in Biot's equations for acoustic waves in fluid-filled porous media*, Geophysics, Vol. 45 (1980), pp. 1269-1275.

[26] COMSOL, Multiphysics user's guide, Comsol AB, v5.1.

[27] S. G. Advani and C. L. Tucker, *The use of tensors to describe and predict fiber orientation in short fiber composites*, Journal of Rheology, Vol. 31 (1987), pp. 751-784.

[28] J.-F. Allard and Y. Champoux, *New empirical equations for sound propagation in rigid frame fibrous materials*, Journal of the Acoustical Society of America, Vol. 91 (1992), pp. 3346-3353.

[29] R. Panneton, *Comments on the limp frame equivalent fluid model for porous media*, Journal of the Acoustical Society of America, Vol. 122 (2007), pp. EL217-EL222.

[30] N. Atalla, R. Panneton, and P. Debergue, *A mixed displacement-pressure formulation for poroelastic materials*, Journal of the Acoustical Society of America, Vol. 104 (1998), pp. 1444-1452.